Journal of the Optical Society of America A
OPTICS, IMAGE SCIENCE, AND VISION

Launching surface plasmon waves via vanishingly small periodic gratings

David P. Nicholls,[1,*] Sang-Hyun Oh,[2] Timothy W. Johnson,[2] and Fernando Reitich[3]

[1]Department of Mathematics, Statistics, and Computer Science, University of Illinois at Chicago, Chicago, Illinois 60607, USA
[2]Department of Electrical and Computer Engineering, University of Minnesota, Minneapolis, Minnesota 55455, USA
[3]CAP S.A., Santiago, Chile
*Corresponding author: davidn@uic.edu

Received 20 October 2015; revised 30 December 2015; accepted 30 December 2015; posted 5 January 2016 (Doc. ID 251574); published 5 February 2016

The scattering of electromagnetic waves by periodic layered media plays a crucial role in many applications in optics and photonics, in particular in nanoplasmonics for topics as diverse as extraordinary optical transmission, photonic crystals, metamaterials, and surface plasmon resonance biosensing. With these applications in mind, we focus on surface plasmon resonances excited in the context of insulator–metal structures with a periodic, corrugated interface. The object of this contribution is to study the geometric limits required to generate these fundamentally important phenomena. For this we use the robust, rapid, and highly accurate field expansions method to investigate these delicate phenomena and demonstrate how very small perturbations (e.g., a 5 nm deviation on a 530 nm period grating) can generate strong (in this instance 20%) plasmonic absorption, and vanishingly small perturbations (e.g., a 1 nm deviation on a 530 nm period grating) can generate nontrivial (in this instance 1%) plasmonic absorption.

OCIS codes: (050.1755) Computational electromagnetic methods; (240.6680) Surface plasmons.

http://dx.doi.org/10.1364/JOSAA.33.000276

1. INTRODUCTION

The scattering of linear electromagnetic waves by periodic layered media plays a crucial role in many applications of scientific and engineering interest. In optics and photonics, for instance, this can be seen in nanoplasmonics [1–3], where one can investigate topics as diverse as extraordinary optical transmission [4,5], photonic crystals [6,7], metamaterials [8], surface acousto-optic systems [9,10], and surface plasmon resonance (SPR) biosensing [11–17].

The objects of our current investigation are the SPRs at the heart of a wide range of highly accurate and robust biosensing devices of current interest (see, e.g., [12]). These SPRs are generated when a surface plasmon polariton (an exponentially confined time-harmonic electromagnetic wave propagating at the interface between an insulator and a metal) is excited and coupled to the illuminating radiation.

A well-known property of these SPRs is that they cannot be excited at the boundary of an insulator–metal structure with a flat interface (though they can be launched in the Kretschmann configuration) [1–3]. It is not difficult to show that there is insufficient "momentum" to generate an SPR. With the addition of periodic corrugations at the interface, such momentum can be provided and SPRs can be excited. (Periodic gratings are among several methods of producing SPRs, and we refer the interested reader to [1–3] for other approaches.)

It is also known that these SPRs can be generated by quite small deformations. The object of this contribution is to study the limits of the size of the deformation required to generate surface plasmon waves. In concert with this, a remarkable feature of these resonances is that for a well-designed (i.e., the metal should be a superior conductor, e.g., having permittivity with a very negative real part) but fixed configuration, they are excited only for a very narrow band of illumination frequencies. Clearly, the ability to simulate such configurations numerically in a rapid, robust, and high-order fashion is of paramount importance.

While all of the classical numerical algorithms have been brought to bear upon this problem, each has shortcomings. Typically one considers methods based on finite elements (see, e.g., [18–21]) and finite differences (see, e.g., [22–24]). However, these volumetric approaches are clearly disadvantaged by an unnecessarily large number of unknowns for the problem at hand, which features piecewise-constant dielectric constants. Methods based on traditional integral equation (IE) formulations [25] are a natural candidate but face several challenges. While most have been adequately addressed with appropriate quadrature rules and iteration procedures (see [26] and [27] for different strategies), the authors recently argued [17,28] that these methods are noncompetitive for the *periodic, parameterized* problems we consider as compared with "high-order perturbation of surfaces" (HOPS) algorithms, which we advocate here.

More specifically, in [17,28] we pointed out that standard IE methods have the following properties:

1. For periodic problems, the relevant Green's function must be periodized if one is to restrict the domain of integration to a single period cell. This is a well-known problem (see, e.g., the introduction of [29] for a full description), and the slow convergence of the periodization must be accelerated (e.g., with techniques such as Ewald summation). However, even with such technology, these IE methods demand an additional discretization parameter: the number of terms retained in the approximation of the periodized Green's function. (We note the recent results [30] and [31], which significantly ameliorate this concern.)
2. For configurations parameterized by the real value h (for us the height/slope of the crossed interface), an IE solver will return the scattering returns only for a particular value of h. If this value is changed, then the solver must be run again.
3. The dense, nonsymmetric positive definite systems of linear equations, which must be inverted with each simulation.

In this contribution we utilize a particular HOPS approach: the method of field expansions (FE), which traces its roots to the low-order calculations of Rayleigh [32] and Rice [33]. Its high-order incarnation for doubly layered media was first introduced by Bruno and Reitich for the two-dimensional scalar case in [34,35] and for the fully three-dimensional vector Maxwell case in [36]. It was further enhanced and stabilized by Nicholls and Reitich [37–39], and expanded to multiple layers in the two-dimensional scalar case by Malcolm and Nicholls [40] and the fully three-dimensional vector electromagnetic case by Nicholls [28].

As we pointed out in [17,28], this formulation is particularly compelling, as it maintains the advantageous properties of classical IE formulations (e.g., surface formulation and exact enforcement of far-field conditions) while avoiding the shortcomings listed above:

1. As this HOPS scheme utilizes the eigenfunctions of the Laplacian (suitable complex exponentials) on a periodic domain, the quasiperiodicity of solutions is built in and does not need to be further approximated.
2. Since the method is built upon expansions in the boundary parameter, h, once the Taylor coefficients are known for the scattering quantities, it is simply a matter of summing these (rather than beginning a new simulation) for any given choice of h to recover the returns.
3. Due to the perturbative nature of the scheme, at every perturbation order one need only invert a single sparse operator corresponding to the flat-interface approximation of the problem.

With this method we can show that vanishingly small-amplitude (e.g., a 5 nm deviation on a 530 nm period grating) perturbations can give rise to substantial plasmonic absorption on the order of a 20% dip from the base, flat-interface return. This is of particular relevance to experimentalists, since the roughness of as-deposited metal films can be on the order of 5 nm, unless ultraflat metal films are produced using techniques such as template stripping [41].

From here the paper is organized as follows: In Section 2 we briefly recall the equations that govern the propagation of electromagnetic waves in a periodic structure that is invariant in one direction, rendering this problem two-dimensional. In Section 3 we specify the method of FE for numerically approximating solutions to these governing equations [28,34–36,40]. In Section 4 we make a simple explanation of the SPR phenomena in terms of the FE framework introduced in Section 3. In Section 5 we discuss our numerical simulations, including the implementation (Section 5.A) and results for vanishingly small perturbations (Section 5.B).

2. GOVERNING EQUATIONS

In Fig. 1 we show the geometry of the configuration we consider: A y-invariant doubly layered insulator–metal structure. The insulator (vacuum with refractive index $n^{(u)} = 1$) occupies the domain *above* the graph $z = g(x)$,

$$S^{(u)} := \{z > g(x)\},$$

and the metal (with index of refraction $n^{(w)}$) fills

$$S^{(w)} := \{z < g(x)\}.$$

The grating is d-periodic so that $g(x + d) = g(x)$. The structure is illuminated from above by monochromatic plane-wave incidence of frequency ω, aligned with the grooves

$$\underline{\mathbf{E}}^i(x, z, t) = \mathbf{A}e^{i\alpha x - i\gamma z - i\omega t}, \underline{\mathbf{H}}^i(x, z, t) = \mathbf{B}e^{i\alpha x - i\gamma z - i\omega t}.$$

We consider the reduced electric and magnetic fields

$$\mathbf{E}(x, z) = e^{i\omega t}\underline{\mathbf{E}}, \mathbf{H}(x, z) = e^{i\omega t}\underline{\mathbf{H}},$$

which, like the reduced scattered fields, are α-quasiperiodic due to the incident radiation. Finally, the scattered radiation must be "outgoing" (upward propagating in $S^{(u)}$ and downward propagating in $S^{(w)}$).

As shown in Petit [42], in this two-dimensional setting, the time-harmonic Maxwell equations decouple into two scalar

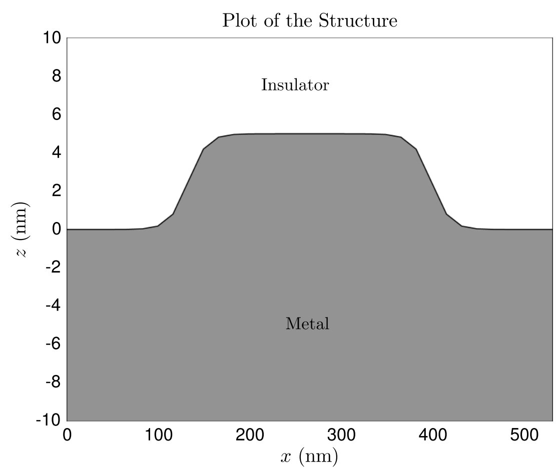

Fig. 1. Plot of an insulator–metal structure with periodic lamellar interface (period $d = 530$ nm and height $h = 5$ nm).

Helmholtz problems that govern the transverse electric (TE) and transverse magnetic (TM) polarizations. We denote the invariant (y) directions of the scattered electric and magnetic fields by

$$u = u(x, z), w = w(x, z),$$

in $S^{(u)}$ and $S^{(w)}$, respectively. The incident radiation in the upper layer is specified by u^i.

In light of all of this, we are led to seek outgoing, α-quasiperiodic solutions of

$$\Delta u + (k^{(u)})^2 u = 0, \qquad z > g(x), \tag{2.1a}$$

$$\Delta w + (k^{(w)})^2 w = 0, \qquad z < g(x), \tag{2.1b}$$

$$u - w = \zeta, \qquad z = g(x), \tag{2.1c}$$

$$\partial_N u - \tau^2 \partial_N w = \psi, \qquad z = g(x), \tag{2.1d}$$

where $k^{(m)} = n^{(m)}\omega/c$, $N = (-\partial_x g, 1)^T$, the Dirichlet and Neumann data are

$$\zeta(x) := -u^i(x, g(x)) = -e^{i\alpha x - i\gamma^{(u)} g(x)},$$

$$\psi(x) := -(\partial_N u^i)(x, g(x)) = (i\gamma^{(u)} + i\alpha(\partial_x g))e^{i\alpha x - i\gamma^{(u)} g(x)},$$

and

$$\tau^2 = \begin{cases} 1 & \text{TE} \\ (k^{(u)}/k^{(w)})^2 = (n^{(u)}/n^{(w)})^2 & \text{TM} \end{cases}.$$

Appealing to the classical study of SPRs [1], we restrict our attention to TM polarization from here.

A. Rayleigh Expansions

Separation of variables gives the Rayleigh expansions [42], which are quasiperiodic, outgoing solutions of Eqs. (2.1a) and (2.1b). The electric fields can be written

$$u(x, z) = \sum_{p=-\infty}^{\infty} \hat{a}_p e^{i\alpha_p x} e^{i\gamma_p^{(u)} z}, \tag{2.2a}$$

$$w(x, z) = \sum_{p=-\infty}^{\infty} \hat{d}_p e^{i\alpha_p x} e^{-i\gamma_p^{(w)} z}, \tag{2.2b}$$

where, for $p \in \mathbf{Z}$ and $m = u, w$,

$$\alpha_p := \alpha + \left(\frac{2\pi}{d}\right)p, \qquad \gamma_p^{(m)} := \begin{cases} \sqrt{(k^{(m)})^2 - \alpha_p^2} & p \in \mathcal{U}^{(m)} \\ i\sqrt{\alpha_p^2 - (k^{(m)})^2} & p \notin \mathcal{U}^{(m)} \end{cases},$$

and

$$\mathcal{U}^{(m)} = \{p \in \mathbf{Z} | \alpha_p^2 < (k^{(m)})^2\},$$

which are the "propagating modes" in the upper and lower layers. We point out that $\hat{a}_p$ and $\hat{d}_p$ are the upward and downward propagating Rayleigh amplitudes. Quantities of great interest are the *efficiencies*

$$e_p^{(u)} = (\gamma_p^{(u)}/\gamma^{(u)})|\hat{a}_p|^2, \qquad e_p^{(w)} = (\gamma_p^{(w)}/\gamma^{(u)})|\hat{d}_p|^2,$$

and the objects of fundamental importance to the design of SPR biosensors [12–17] are the "reflectivity map" and "normalized reflectivity,"

$$R := \sum_{p \in \mathcal{U}^{(u)}} e_p^{(u)}, \qquad B(\lambda, h) := \frac{e_0^{(u)}(\lambda, h)}{e_0^{(u)}(\lambda, 0)}, \tag{2.3}$$

respectively. If the lower layer is filled with a perfect electric conductor, then if $S^{(u)}$ contains an insulator (such as the vacuum), conservation of energy requires that $R = 1$. This is *not* the case for a metal (such as gold or silver) in the lower domain, and drops in its value to a tenth or even a hundredth are the fundamental phenomena behind the utility of these sensors.

3. FIELD EXPANSIONS

The method of FE [34–36] is a perturbative approach to enforcing the boundary conditions in Eqs. (2.1c) and (2.1d) with the $\{\hat{a}_p, \hat{d}_p\}$ from the Rayleigh expansions in Eq. (2.2) as unknowns. Here we take the point of view advocated by one of the authors in [28], which, we believe, simplifies the presentation. First, we define the functions

$$a(x) := u(x, 0) = \sum_{p=-\infty}^{\infty} \hat{a}_p e^{i\alpha_p x} \tag{3.1a}$$

$$d(x) := w(x, 0) = \sum_{p=-\infty}^{\infty} \hat{d}_p e^{i\alpha_p x}, \tag{3.1b}$$

which are the "flat interface" field traces.

We further define the Dirichlet trace operators

$$\mathcal{D}^{(u)}: a \to u(x, g(x)), \qquad \mathcal{D}^{(w)}: d \to w(x, g(x)),$$

and their Neumann counterparts

$$\mathcal{N}^{(u)}: a \to (\partial_z u - (\partial_x g)\partial_x u)(x, g(x)),$$

$$\mathcal{N}^{(w)}: d \to (\partial_z w - (\partial_x g)\partial_x w)(x, g(x)).$$

The idea behind these operators $\mathcal{D}$ and $\mathcal{N}$ is that they map, respectively, the function pair (a, d) to the upper and lower Dirichlet and Neumann traces. It can be shown that

$$\mathcal{D}^{(u)} = \exp(g(i\gamma_D^{(u)})), \qquad \mathcal{D}^{(w)} = \exp(g(-i\gamma_D^{(w)})),$$

and

$$\mathcal{N}^{(u)} = \exp(g(i\gamma_D^{(u)}))(i\gamma_D^{(u)}) - (\partial_x g)\exp(g(i\gamma_D^{(u)}))\partial_x,$$

$$\mathcal{N}^{(w)} = \exp(g(-i\gamma_D^{(w)}))(-i\gamma_D^{(w)}) - (\partial_x g)\exp(g(-i\gamma_D^{(w)}))\partial_x,$$

where we have used Fourier multiplier notation, e.g.,

$$m(D)\xi(x) := \sum_{p=-\infty}^{\infty} m(p)\hat{\xi}_p e^{i\alpha_p x},$$

where $\hat{\xi}_p$ is the generalized pth Fourier coefficient of $\xi(x)$.

In these terms, the Dirichlet boundary condition, Eq. (2.1c), becomes

$$\mathcal{D}^{(u)}[a] - \mathcal{D}^{(w)}[d] = \zeta, \tag{3.2}$$

while the Neumann condition, Eq. (2.1d), becomes

$$\mathcal{N}^{(u)}[a] - \tau^2 \mathcal{N}^{(w)}[d] = \psi. \tag{3.3}$$

We state the boundary conditions [Eqs. (3.2) and (3.3)] abstractly as

$$\mathbf{Mv} = \mathbf{b}, \tag{3.4}$$

where

$$\mathbf{M} = \begin{pmatrix} \mathcal{D}^{(u)} & \mathcal{D}^{(w)} \\ \mathcal{N}^{(u)} & -\tau^2\mathcal{N}^{(w)} \end{pmatrix}, \quad \mathbf{v} = \begin{pmatrix} a \\ d \end{pmatrix}, \quad \mathbf{b} = \begin{pmatrix} \zeta \\ \psi \end{pmatrix}.$$

A. Taylor Expansions

The FE approach to this problem is to consider deformations of the form $g(x) = hf(x)$ ($f = \mathcal{O}(1)$) and note that for a sufficiently smooth f (Lipschitz) and sufficiently small h, the linear operator $\mathbf{M}$ and inhomogeneity $\mathbf{b}$ are both analytic in h [43,44]. Furthermore, an analytic solution $\mathbf{v}$ can be shown to exist. More specifically, the following expansions can be demonstrated to be strongly convergent:

$$\{\mathbf{M}, \mathbf{v}, \mathbf{b}\}(hf) = \sum_{n=0}^{\infty}\{\mathbf{M}_n(f), \mathbf{v}_n(f), \mathbf{b}_n(f)\}h^n.$$

Crucially, an algorithm for recovering $\mathbf{v}_n$ can be devised based on regular perturbation theory. In short, we write Eq. (3.4) as

$$\left(\sum_{n=0}^{\infty}\mathbf{M}_n h^n\right)\left(\sum_{m=0}^{\infty}\mathbf{v}_m h^m\right) = \sum_{n=0}^{\infty}\mathbf{b}_n h^n,$$

and, equating at each perturbation order, we find

$$\mathbf{M}_0\mathbf{v}_n = \mathbf{b}_n - \sum_{m=0}^{n-1}\mathbf{M}_{n-m}\mathbf{v}_m. \tag{3.5}$$

At order zero we recover the flat-interface solution, giving the Fresnel coefficients, while higher-order corrections, $\mathbf{v}_n$, can be computed by appealing to Eq. (3.5). Of great importance is the fact that one only need invert the *same* linear operator, $\mathbf{M}_0$, at *every* perturbation order. All that remains is a specification of the terms $\{\mathbf{M}_n, \mathbf{b}_n\}$.

Regarding the Dirichlet trace operators, upon defining

$$F_n(x) := f(x)^n/n!,$$

one can show that

$$\mathcal{D}_n^{(u)} = F_n(i\gamma_D^{(u)})^n, \qquad \mathcal{D}_n^{(w)} = F_n(-i\gamma_D^{(w)})^n.$$

For their Neumann counterparts, we have

$$\mathcal{N}_n^{(u)} = F_n(i\gamma_D^{(u)})^{n+1} - (\partial_x f)F_{n-1}\partial_x(i\gamma_D^{(u)})^{n-1},$$
$$\mathcal{N}_n^{(w)} = F_n(-i\gamma_D^{(w)})^{n+1} - (\partial_x f)F_{n-1}\partial_x(-i\gamma_D^{(w)})^{n-1}.$$

Finally, for the surface data, $\mathbf{b}_n$, it is easy to show that

$$\zeta_n = -F_n(-i\gamma^{(u)})^n e^{i\alpha x},$$

and

$$\psi_n = F_n(i\gamma^{(u)})(-i\gamma^{(u)})^n e^{i\alpha x} + (\partial_x f)F_{n-1}(i\alpha)(-i\gamma^{(u)})^{n-1}e^{i\alpha x},$$

where $F_{-1}(x) \equiv 0$ and $F_0(x) \equiv 1$.

4. PERSISTENCE OF SPRS AT VANISHINGLY SMALL AMPLITUDE

The SPR phenomena have been observed since the time of Wood [45], and explanations for the onset of these surface waves for extremely narrow bands of illumination wavelengths can be traced to the foundational work of Rayleigh [32] (see the fascinating article of Maystre in Chapter 1 of [3]). This is all discussed in a number of sources including the books of Raether [1], Maier [2], and Novotny and Hecht [3]. Here we recover these results in the language of the boundary formulation [Eq. (3.4)] and the FE approach.

The onset of an SPR is indicated by a precipitous drop in the normalized reflectivity, B [Eq. (2.3)], as a function of λ. In the current formulation,

$$B(\lambda, h) = 1 + B_1(\lambda)h + B_2(\lambda)h^2 + \mathcal{O}(h^3),$$

where

$$B_1 = \frac{\hat{a}_{0,1}\overline{\hat{a}_{0,0}} + \hat{a}_{0,0}\overline{\hat{a}_{0,1}}}{|\hat{a}_{0,0}|^2},$$

and

$$B_2 = \frac{\hat{a}_{0,2}\overline{\hat{a}_{0,0}} + \hat{a}_{0,1}\overline{\hat{a}_{0,1}} + \hat{a}_{0,0}\overline{\hat{a}_{0,2}}}{|\hat{a}_{0,0}|^2}.$$

We will now demonstrate that $B_1 \equiv 0$, while B_2 takes on very large negative values at an SPR.

To simplify the presentation, we use the notation

$$U := (i\gamma_D^{(u)}), \qquad W := (-i\gamma_D^{(w)}), \qquad Z := (-i\gamma^{(u)}),$$

and further fix upon normally incident illumination so that $\alpha = 0$. With these, we have

$$\mathcal{D}_n^{(u)} = F_n U^n, \qquad \mathcal{D}_n^{(w)} = F_n W^n,$$
$$\mathcal{N}_n^{(u)} = F_n U^{n+1} - (\partial_x f)F_{n-1}\partial_x U^{n-1},$$
$$\mathcal{N}_n^{(w)} = F_n W^{n+1} - (\partial_x f)F_{n-1}\partial_x W^{n-1},$$
$$\zeta_n = -F_n Z^n, \qquad \psi_n = -F_n Z^{n+1},$$

which gives

$$\mathbf{M}_0 = \begin{pmatrix} I & -I \\ U & -\tau^2 W \end{pmatrix}, \qquad \mathbf{b}_0 = -\begin{pmatrix} 1 \\ Z \end{pmatrix},$$

and

$$\mathbf{M}_n = F_n\begin{pmatrix} U^n & -W^n \\ U^{n+1} & -\tau^2 W^{n+1} \end{pmatrix} - (\partial_x f)F_{n-1}\partial_x\begin{pmatrix} 0 & 0 \\ U^{n-1} & \tau^2 W^{n-1} \end{pmatrix},$$

$$\mathbf{b}_n = -F_n Z^n\begin{pmatrix} 1 \\ Z \end{pmatrix}.$$

For future reference, it can be shown that

$$\mathbf{M}_0^{-1} = \Delta^{-1}\begin{pmatrix} -\tau^2 W & I \\ -U & I \end{pmatrix},$$

where $\Delta := U - \tau^2 W$, and

$$\Delta^{-1}[e^{i\tilde{p}x}] = \left(\frac{1}{\hat{\Delta}_p}\right)e^{i\tilde{p}x},$$

where $\hat{\Delta}_p := i\gamma_p^{(u)} + i\tau^2\gamma_p^{(w)}$ and $\tilde{p} := (2\pi/d)p$.

A. Order Zero: Fresnel Coefficients

At order zero, Eq. (3.4) delivers

$$\begin{pmatrix} a_0 \\ d_0 \end{pmatrix} = \mathbf{v}_0 = \mathbf{M}_0^{-1}\mathbf{b}_0 = -\Delta^{-1}\begin{pmatrix} -\tau^2 W & I \\ -U & I \end{pmatrix}\begin{pmatrix} 1 \\ Z \end{pmatrix}$$
$$= -\Delta^{-1}\begin{pmatrix} -\tau^2 W[1] + Z \\ -U[1] + Z \end{pmatrix}.$$

Recalling that

$$U[1] = (i\gamma^{(u)}), \qquad W[1] = (-i\gamma^{(w)}),$$

we find the solutions

$$a_0(x,z) = Re^{i\gamma^{(u)}z}, \qquad d_0(x,z) = Te^{-i\gamma^{(w)}z}, \tag{4.1}$$

with the Fresnel (reflection and transmission) coefficients

$$R = \frac{i\gamma^{(u)} - \tau^2 i\gamma^{(w)}}{\hat{\Delta}_0}, \qquad T = \frac{2i\gamma^{(u)}}{\hat{\Delta}_0}.$$

There is no appreciable variation in R as λ is varied; one requires $f \not\equiv 0$ to find an SPR.

B. Order One: B_1

At order one, Eq. (3.4) becomes

$$\mathbf{M}_0\mathbf{v}_1 = \mathbf{b}_1 - \mathbf{M}_1\mathbf{v}_0 =: \mathbf{S}_1,$$

where

$$\mathbf{b}_1 = -fZ\begin{pmatrix} 1 \\ Z \end{pmatrix},$$

and

$$\mathbf{M}_1 = f\begin{pmatrix} U & -W \\ U^2 & -\tau^2 W^2 \end{pmatrix} - (\partial_x f)\partial_x\begin{pmatrix} 0 & 0 \\ I & -\tau^2 I \end{pmatrix},$$

so that

$$\mathbf{S}_1 = f\begin{pmatrix} (1-R)(i\gamma^{(u)}) - T(i\gamma^{(w)}) \\ -(1+R)(i\gamma^{(u)})^2 + T\tau^2(-i\gamma^{(w)})^2 \end{pmatrix}.$$

We seek solutions of the form

$$a_1(x) = \sum_{p=-\infty}^{\infty} \hat{a}_{1,p}e^{i\tilde{p}x}, \qquad d_1(x) = \sum_{p=-\infty}^{\infty} \hat{d}_{1,p}e^{i\tilde{p}x},$$

which has the solution

$$\begin{pmatrix} \hat{a}_{1,p} \\ \hat{d}_{1,p} \end{pmatrix} = \mathbf{M}_0^{-1}\widehat{(\mathbf{S}_1)}_p = \frac{\hat{f}_p}{\hat{\Delta}_p}\begin{pmatrix} \tilde{R}_p \\ \tilde{T}_p \end{pmatrix}.$$

It is not difficult to show that

$$\tilde{R}_p = -(\tau^2(i\gamma_p^{(w)}) + Z)Z - (\tau^2(i\gamma_p^{(w)}) + i\gamma^{(u)})(i\gamma^{(u)})R + (-(i\gamma_p^{(w)}) + (i\gamma^{(w)}))\tau^2(i\gamma^{(w)})T,$$

and

$$\tilde{T}_p = ((i\gamma_p^{(u)}) - Z)Z + ((i\gamma_p^{(u)}) - (i\gamma^{(u)}))(i\gamma^{(u)})R + ((i\gamma_p^{(u)}) + \tau^2(i\gamma^{(w)}))(i\gamma^{(w)})T.$$

Importantly, since the mean of f is zero, we have $\hat{f}_0 = 0$, so that $\hat{a}_{1,0} = \hat{d}_{1,0} = 0$, which implies that

$$B_1 \equiv 0.$$

We must move to order two to see the SPR.

C. Order Two: B_2

At order two, Eq. (3.4) becomes

$$\mathbf{M}_0\mathbf{v}_2 = \mathbf{b}_2 - \mathbf{M}_1\mathbf{v}_1 - \mathbf{M}_2\mathbf{v}_0 =: \mathbf{S}_2,$$

where

$$\mathbf{b}_2 = -\frac{1}{2}f^2Z^2\begin{pmatrix} 1 \\ Z \end{pmatrix},$$

and

$$\mathbf{M}_2 = \frac{1}{2}f^2\begin{pmatrix} U^2 & -W^2 \\ U^3 & -\tau^2 W^3 \end{pmatrix} - (\partial_x f)f\partial_x\begin{pmatrix} 0 & 0 \\ U & -\tau^2 W \end{pmatrix}.$$

Again, we seek solutions of the form

$$a_2(x) = \sum_{p=-\infty}^{\infty} \hat{a}_{2,p}e^{i\tilde{p}x}, \qquad d_2(x) = \sum_{p=-\infty}^{\infty} \hat{d}_{2,p}e^{i\tilde{p}x},$$

which can be solved to yield

$$\begin{pmatrix} \hat{a}_{2,p} \\ \hat{d}_{2,p} \end{pmatrix} = \mathbf{M}_0^{-1}\widehat{(\mathbf{S}_2)}_p = \sum_{q=-\infty}^{\infty} \hat{f}_{p-q}\hat{f}_q\begin{pmatrix} \underline{R}_{p,q} \\ \underline{T}_{p,q} \end{pmatrix}.$$

Unfortunately, the forms for $\{\underline{R}_{p,q}, \underline{T}_{p,q}\}$ are rather unwieldy and we do not report them here. However, there are a few things one can say.

Our goal is to investigate the nature of the SPR and the role played by the classic condition [1–3]

$$\hat{\Delta}_1 \approx 0.$$

For this we focus on $\mathbf{S}_2$, and since the determinant of $\mathbf{M}_0$ at wavenumber $p = 0$ ($\hat{\Delta}_0$) is of order one, we seek near-singularities in this right-hand side to generate the dramatic SPR response. We note that $\mathbf{b}_2$ and $\mathbf{M}_2\mathbf{v}_0$ are also of order one throughout the range of λ, and thus we focus on $\mathbf{M}_1\mathbf{v}_1$. In Fourier space it can be shown that

$$\widehat{(\mathbf{M}_1\mathbf{v}_1)}_p = \sum_{q=-\infty}^{\infty} \hat{f}_{p-q}\hat{f}_q\begin{pmatrix} \hat{\xi}_q/\hat{\Delta}_p \\ \hat{\nu}_q/\hat{\Delta}_p + i(p-q)\hat{\kappa}_q/\hat{\Delta}_p \end{pmatrix},$$

where

$$\hat{\xi}_p := (i\gamma_p^{(u)})\tilde{R}_p + (i\gamma_p^{(w)})\tilde{T}_p,$$
$$\hat{\nu}_p := (i\gamma_p^{(u)})^2\tilde{R}_p - \tau^2(i\gamma_p^{(w)})^2\tilde{T}_p,$$
$$\hat{\kappa}_p := -(ip)\tilde{R}_p + \tau^2(ip)\tilde{T}_p.$$

Importantly, while $\hat{f}_0 = 0$, $\hat{f}_1 \neq 0$ generically, so that contributions to $\widehat{(\mathbf{M}_1\mathbf{v}_1)}_1$ will come from $\hat{\xi}_1/\hat{\Delta}_1$, $\hat{\nu}_1/\hat{\Delta}_1$, and $\hat{\kappa}_1/\hat{\Delta}_1$.

We summarize our findings:

1. In Fig. 2 we see that the denominator of $\widehat{(\mathbf{M}_1\mathbf{v}_1)}_1$, $|\hat{\Delta}_1|^2$, approaches zero very rapidly as λ tends towards the SPR value $\lambda_{\mathrm{SPR}} \approx 557.4$ nm, while being far from zero near the "passing-off value" (which we denote as the Rayleigh value $\lambda_{\mathrm{Ray}} = d = 530$ nm).
2. In Fig. 3 we plot three components of the numerator of $\widehat{(\mathbf{M}_1\mathbf{v}_1)}_1$,
$$\{|\hat{\xi}_1|^2, |\hat{\nu}_1|^2, |\hat{\kappa}_1|^2\},$$
versus λ. Two of these tend to zero as λ approaches λ_{Ray}, while all three vary quite continuously (and none become particularly large) as λ changes.
3. By contrast, in Fig. 4 we display three components of $\widehat{(\mathbf{M}_1\mathbf{v}_1)}_1$,
$$\{|\hat{\xi}_1/\hat{\Delta}_1|^2, |\hat{\nu}_1/\hat{\Delta}_1|^2, |\hat{\kappa}_1/\hat{\Delta}_1|^2\},$$
versus λ. Two of these tend to zero as $\lambda \to \lambda_{\mathrm{Ray}}$, but all three become anomalously large as $\lambda \to \lambda_{\mathrm{SPR}}$. From this it becomes

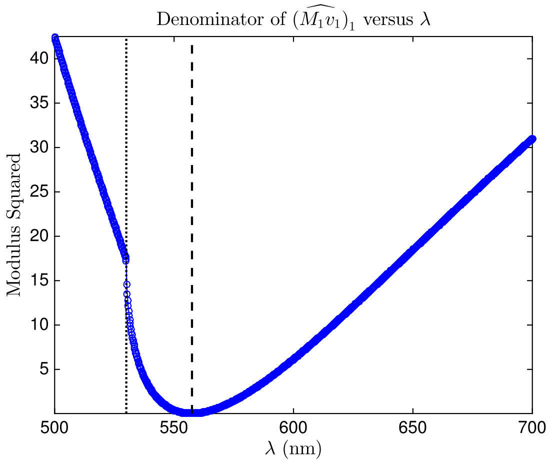

Fig. 2. Second-order correction of the normalized reflectivity: plot of the denominator of $(\widehat{\mathbf{M}_1\mathbf{v}_1})_1$, one of three components of the second correction to the normalized reflectivity, B, as a function of incident wavelength λ. Dotted line at $\lambda = \lambda_{\text{Ray}}$ and dashed line at $\lambda = \lambda_{\text{SPR}}$. Note the nonvanishing value at λ_{Ray} but near-zero value at λ_{SPR}.

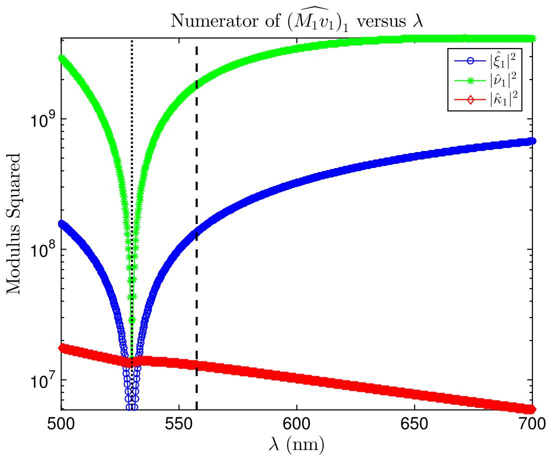

Fig. 3. Second-order correction of the normalized reflectivity: plot of the numerator of $(\widehat{\mathbf{M}_1\mathbf{v}_1})_1$, one of three components of the second correction to the normalized reflectivity, B, as a function of incident wavelength λ. Dotted line at $\lambda = \lambda_{\text{Ray}}$ and dashed line at $\lambda = \lambda_{\text{SPR}}$. Note the relatively modest values at both λ_{Ray} and λ_{SPR}, where the values vary continuously.

clear that the *only* reason for the SPR in terms of these equations is the near-zero value of $\hat{\Delta}_1$ at λ_{SPR}.

While it is difficult to explain all of the constituent parts of $\hat{a}_{2,0}$, and therefore B_2, we can say that it depends linearly upon

$$\{\hat{\xi}_1/\hat{\Delta}_1, \hat{\nu}_1/\hat{\Delta}_1, \hat{\kappa}_1/\hat{\Delta}_1\}.$$

In this way we see quite explicitly how at very low (second) order, the SPR condition $\hat{\Delta}_1 \approx 0$ can generate its remarkably strong and specific effect.

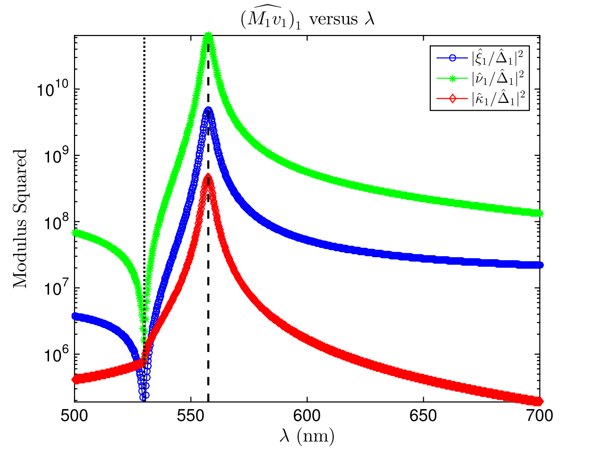

Fig. 4. Second-order correction of the normalized reflectivity: plot of $(\widehat{\mathbf{M}_1\mathbf{v}_1})_1$, one of three components of the second correction to the normalized reflectivity, B, as a function of incident wavelength λ. Dotted line at $\lambda = \lambda_{\text{Ray}}$ and dashed line at $\lambda = \lambda_{\text{SPR}}$. Note the relatively modest values at λ_{Ray}, while all three values grow anomalously as λ approaches λ_{SPR}.

5. NUMERICAL RESULTS

We are now in a position to explore the conclusions above for the case of a *very* small perturbation of an ultraflat silver interface. In these we investigate deformations with a size on the order of the roughness of as-deposited metal films (approximately 5 nm on a grating of period 530 nm) in the absence of specialized deposition techniques [41].

A. Numerical Implementation

The method described in Section 3 is essentially a Fourier collocation [46]/Taylor method [37,47] enhanced by Padé approximation [44,48]. More specifically, we approximate the fields $\{u, w\}$ by

$$u^{N_x,N} := \sum_{n=0}^{N} \sum_{p=-N_x/2}^{N_x/2-1} \hat{a}_{n,p} e^{i\alpha_p x} e^{i\gamma_p^{(u)} z} h^n, \qquad \textbf{(5.1a)}$$

$$w^{N_x,N} := \sum_{n=0}^{N} \sum_{p=-N_x/2}^{N_x/2-1} \hat{d}_{n,p} e^{i\alpha_p x} e^{-i\gamma_p^{(w)} z} h^n \qquad \textbf{(5.1b)}$$

[cf. Eq. (2.2)]. We insert these into Eq. (3.5) and determine $\{\mathbf{v}_n\}$.

A crucial consideration is how the Taylor series in h are summed. To be specific, to approximate u we consider the truncation $u^{N_x,N}$, which amounts to the approximation $\hat{a}_p(h) := \sum_{n=0}^{\infty} \hat{a}_{n,p} h^n$ by $\hat{a}_p^N(h) := \sum_{n=0}^{N} \hat{a}_{n,p} h^n$. The classical numerical analytic continuation technique of Padé approximation [48] has been successfully brought to bear upon HOPS methods in the past (see, e.g., [28,35,44]), and we advocate its use here. Padé approximation seeks to simulate the truncated Taylor series $\hat{a}_p^N(h)$ by the rational function

$$[L/M](h) := \frac{A^L(h)}{B^M(h)} = \frac{\sum_{\ell=0}^{L} A_\ell h^\ell}{1 + \sum_{m=1}^{M} B_m h^m}, \qquad \textbf{(5.2)}$$

where $L + M = N$ and

$$[L/M](h) = \hat{a}_p^N(h) + \mathcal{O}(h^{L+M+1});$$

well-known formulas for the coefficients $\{A_\ell, B_m\}$ can be found in [48]. This approximant has remarkable properties of enhanced convergence, and we refer the interested reader to Section 2.2 of Baker and Graves-Morris [48] and the insightful calculations of Section 8.3 of Bender and Orszag [49] for a thorough discussion of the capabilities and limitations of Padé approximants.

B. Small Perturbations

We now display results that show that SPRs can be launched for surface profiles with amplitudes on the order of the roughness of as-deposited metal films. To illustrate this, we consider a doubly layered structure of vacuum (an insulator) above silver (a metal), separated by the profile $g(x) = hf(x)$.

To begin, we consider $f(x) = -(1/2)\cos(2\pi x/d)$; see Fig. 5. By definition, the refractive index of vacuum is $n^u = 1$, while the refractive index of silver is still the subject of current research. For this we use a Lorenz model [50],

$$\epsilon^{Ag} = \epsilon_\infty^{Ag} + \sum_{j=1}^{6} \frac{\Delta_j^{Ag}}{-a_j^{Ag}\omega^2 - ib_j^{Ag}\omega + c_j^{Ag}},$$

where $\omega = 2\pi/\lambda$, $\epsilon_\infty^{Ag} = 1$, and Δ^{Ag}, a^{Ag}, b^{Ag}, and c^{Ag} can be found in [50]. For physical and numerical parameters we choose

$$\alpha = 0, \qquad \gamma = (\gamma^v, \gamma^{Ag})^T, \tag{5.3a}$$

$$h = 0, \ldots, 5, \qquad d = 530, \tag{5.3b}$$

$$N_x = 32, \qquad N = 2. \tag{5.3c}$$

In Fig. 6 we display the normalized reflectivity, $B(\lambda, h)$ [cf. Eq. (2.3)], for this configuration, which shows a strong 13% plasmonic response for a perturbation of size 5 nm (<1% of d).

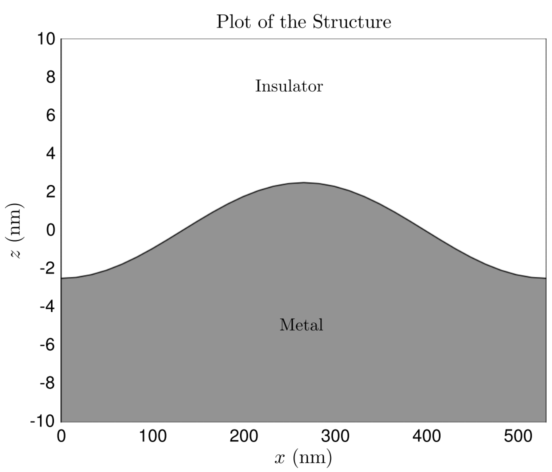

Fig. 5. Plot of an insulator–metal structure with cosine interface (period $d = 530$ nm and height $h = 5$ nm).

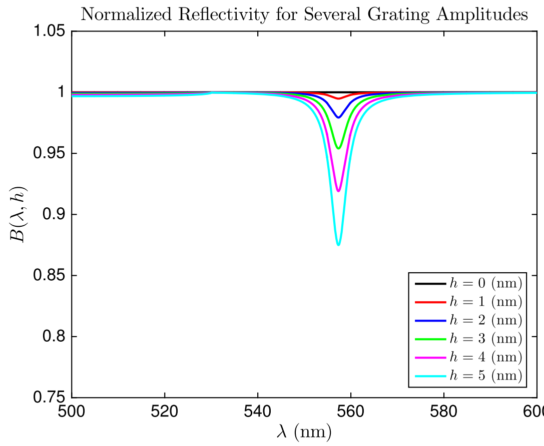

Fig. 6. Normalized reflectivity $B(\lambda, h)$ [Eq. (2.3)] as a function of incident wavelength λ for several grating amplitudes h separating a vacuum–silver interface. Results for the cosine configuration [Eq. (5.3)], with $N_x = 32$, $N = 2$.

We also consider the "lamellar" profile (see Fig. 1),

$$f(x) = \frac{1}{2}\left\{\tanh\left[\sigma\left(x - \frac{d}{2}\right) + \frac{W}{2}\right] - \tanh\left[\sigma\left(x - \frac{d}{2}\right) - \frac{W}{2}\right]\right\};$$

in this, W is the linewidth and σ measures the "steepness" of the line. For instance, in Fig. 1 we chose $\sigma = 50$, $d = 530$ nm, and $W = d/2$. For physical and numerical parameters we choose

$$\alpha = 0, \qquad \gamma = (\gamma^v, \gamma^{Ag})^T, \tag{5.4a}$$

$$h = 0, \ldots, 5, \qquad d = 530, \qquad W = d/2, \tag{5.4b}$$

$$N_x = 32, \qquad N = 2. \tag{5.4c}$$

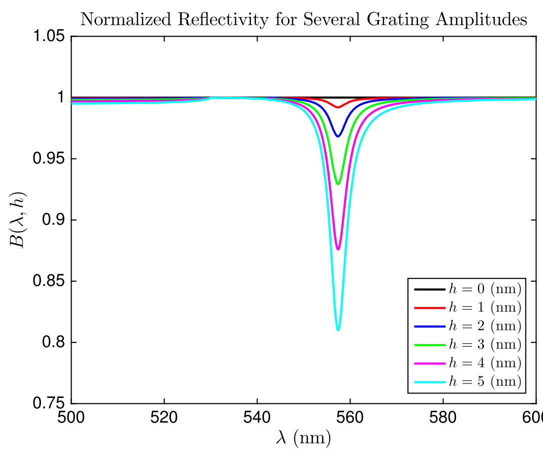

Fig. 7. Normalized reflectivity $B(\lambda, h)$ [Eq. (2.3)] as a function of incident wavelength λ for several grating amplitudes h separating a vacuum–silver interface. Results for the lamellar configuration [Eq. (5.4)], with $N_x = 32$, $N = 2$.

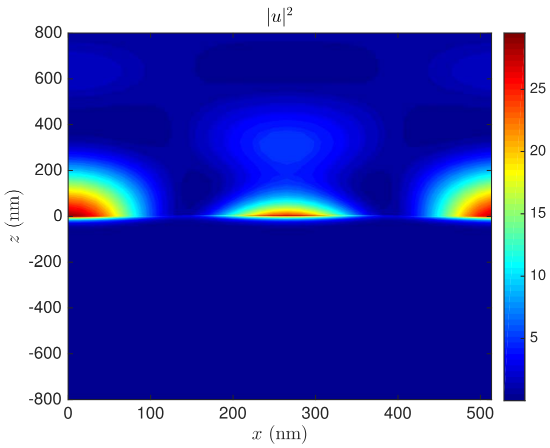

Fig. 8. Plot of the squared norm of the field $|u|^2$ in the lamellar configuration [Eq. (5.4)] at $\lambda = 557.4 \approx \lambda_{\mathrm{SPR}}$, with $N_x = 32$, $N = 2$.

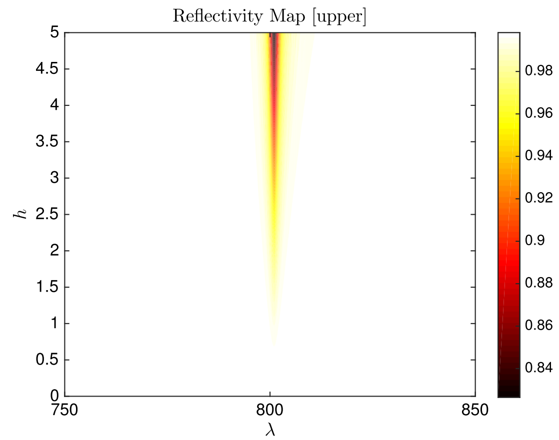

Fig. 9. Reflectivity map $R(\lambda, h)$ [cf. Eq. (2.3)] versus incident wavelength λ and deformation height h. Results for the lamellar configuration [Eq. (5.4)] with grating period $d = 785$ nm and $N_x = 32$, $N = 2$.

Table 1. Numerical Values of the Normalized Reflectivity B [Eq. (2.3)] for $\lambda = 557.4$ nm $\approx \lambda_{\mathrm{SPR}}$ for the Cosine and Lamellar Profiles of Period $d = 530$ nm

h (nm)	Cosine Profile	Lamellar Profile
0	1	1
1	0.994839	0.992012
2	0.979436	0.968234
3	0.954031	0.929244
4	0.919026	0.876019
5	0.874981	0.809930

Table 2. Numerical Values of the Normalized Reflectivity B [Eq. (2.3)] for $\lambda = 682.8$ nm $\approx \lambda_{\mathrm{SPR}}$ for the Cosine and Lamellar Profiles of Period $d = 633$ nm

h (nm)	Cosine Profile	Lamellar Profile
0	1	1
1	0.994977	0.992139
2	0.979984	0.968749
3	0.955248	0.930404
4	0.921149	0.878058
5	0.878219	0.813045

In Fig. 7 we display the normalized reflectivity, $B(\lambda, h)$ [cf. Eq. (2.3)], for this configuration, which shows a strong 20% plasmonic response for a perturbation of size 5 nm (<1% of d).

Table 3. Numerical Values of the Normalized Reflectivity B [Eq. (2.3)] for $\lambda = 801.0$ nm $\approx \lambda_{\mathrm{SPR}}$ for the Cosine and Lamellar Profiles of Period $d = 785$ nm

h (nm)	Cosine Profile	Lamellar Profile
0	1	1
1	0.995426	0.992743
2	0.981766	0.971126
3	0.959209	0.935622
4	0.92807	0.887027
5	0.888791	0.82646

In Fig. 8 we display the squared norm of the field $|u|^2$ in the lamellar configuration at $\lambda = 557.4 \approx \lambda_{\mathrm{SPR}}$. Here the strong plasmonic response for $h = 5$ nm is reflected by the remarkable *confinement* displayed by the scattered field.

In Table 1 we report the numerical values of $B(\lambda, h)$ for $\lambda = 557.4$ nm $\approx \lambda_{\mathrm{SPR}}$ for the cosine and lamellar profiles of period $d = 530$ nm. To help illustrate that these effects are quite robust, we now display results for gratings of different periods, $d = 633$ and 785 nm. In Table 2 we report the numerical values of $B(\lambda, h)$ for $\lambda = 682.8$ nm $\approx \lambda_{\mathrm{SPR}}$ for the cosine and lamellar profiles of period $d = 633$ nm. In Table 3 we report the numerical values of $B(\lambda, h)$ for $\lambda = 801.0$ nm $\approx \lambda_{\mathrm{SPR}}$ for the cosine and lamellar profiles of period $d = 785$ nm. In Fig. 9 we display the normalized reflectivity map, $R(\lambda, h)$ [cf. Eq. (2.3)], for the lamellar configuration [Eq. (5.4)] with grating period $d = 785$ nm. This plot shows both the wavelength λ and deformation height h dependence of the plasmonic response near $\lambda = 801.0$ nm $\approx \lambda_{\mathrm{SPR}}$.

6. CONCLUSION

In this contribution we studied the limits of the surface deformation required to generate SPRs. We explicitly identified the crucial role that the SPR condition, $\hat{\Delta}_1 \approx 0$, plays in this phenomena. Additionally, we used the robust, rapid, and highly accurate FE method to investigate this delicate phenomenon, which is difficult to perform using conventional finite difference time domain or finite element methods due to the low accuracy and exorbitant computational cost of these algorithms. We demonstrated how very small perturbations (e.g., a 5 nm deviation on a 530 nm period grating) can generate strong (in this instance 20%) plasmonic absorption, and vanishingly small perturbations (e.g., a 1 nm deviation on a 530 nm period grating) can generate nontrivial (in this instance 1%) plasmonic absorption. Our findings support the contention that ultrasmooth metal surfaces (roughness on the order of 1 nm or below) can improve the performance of plasmonic resonators, and provide the means to quantitatively explore such experiments.

Funding. National Science Foundation (NSF) (DMS-1115333, DMS-1522548, CMMI-1363334).

Acknowledgment. D.P.N. gratefully acknowledges support from the National Science Foundation through grants DMS-1115333 and DMS-1522548. S.-H.O. and T.W.J. acknowledge support from the National Science Foundation through an NSF CAREER award and grant CMMI-1363334.

REFERENCES

1. H. Raether, *Surface Plasmons on Smooth and Rough Surfaces and on Gratings* (Springer, 1988).
2. S. A. Maier, *Plasmonics: Fundamentals and Applications* (Springer, 2007).
3. L. Novotny and B. Hecht, *Principles of Nano-Optics*, 2nd ed. (Cambridge University, 2012).
4. T. W. Ebbesen, H. J. Lezec, H. F. Ghaemi, T. Thio, and P. A. Wolff, "Extraordinary optical transmission through sub-wavelength hole arrays," Nature **391**, 667–669 (1998).
5. F. J. Garcia-Vidal, L. Martin-Moreno, T. W. Ebbesen, and L. Kuipers, "Light passing through subwavelength apertures," Rev. Mod. Phys. **82**, 729–787 (2010).
6. J. D. Joannopoulos, P. R. Villeneuve, and S. Fan, "Photonic crystals: putting a new twist on light," Nature **386**, 143–149 (1997).
7. Y. A. Vlasov, X.-Z. Bo, J. C. Sturm, and D. J. Norris, "On-chip natural assembly of silicon photonic bandgap crystals," Nature **414**, 289–293 (2001).
8. T. Xu, A. Agrawal, M. Abashin, K. J. Chau, and H. J. Lezec, "All-angle negative refraction and active flat sensing of ultravoilet light," Nature **497**, 470–474 (2013).
9. S. Tadesse and M. Li, "Sub-optical wavelength acoustic wave modulation of integrated photonic resonators at microwave frequencies," Nat. Commun. **5**, 5402–5409 (2014).
10. C. Ruppert, F. Forster, A. Zrenner, J. Kinzel, A. Wixforth, H. Krenner, and M. Betz, "Radio frequency electromechanical control over a surface plasmon polariton coupler," ACS Photon. **1**, 91–95 (2014).
11. A. G. Brolo, R. Gordon, B. Leathem, and K. L. Kavanagh, "Surface plasmon sensor based on the enhanced light transmission through arrays of nanoholes in gold films," Langmuir **20**, 4813–4815 (2004).
12. J. Homola, "Surface plasmon resonance sensors for detection of chemical and biological species," Chem. Rev. **108**, 462–493 (2008).
13. H. Im, S. H. Lee, N. J. Wittenberg, T. W. Johnson, N. C. Lindquist, P. Nagpal, D. J. Norris, and S.-H. Oh, "Template-stripped smooth Ag nanohole arrays with silica shells for surface plasmon resonance biosensing," ACS Nano **5**, 6244–6253 (2011).
14. N. C. Lindquist, T. W. Johnson, J. Jose, L. M. Otto, and S.-H. Oh, "Ultrasmooth metallic films with buried nanostructures for backside reflection-mode plasmonic biosensing," Ann. Phys. **524**, 687–696 (2012).
15. J. Jose, L. R. Jordan, T. W. Johnson, S. H. Lee, N. J. Wittenberg, and S.-H. Oh, "Topographically flat substrates with embedded nanoplasmonic devices for biosensing," Adv. Funct. Mater. **23**, 2812–2820 (2013).
16. F. Reitich, T. W. Johnson, S.-H. Oh, and G. Meyer, "A fast and high-order accurate boundary perturbation method for characterization and design in nanoplasmonics," J. Opt. Soc. Am. A **30**, 2175–2187 (2013).
17. D. P. Nicholls, F. Reitich, T. W. Johnson, and S.-H. Oh, "Fast high-order perturbation of surfaces (HOPS) methods for simulation of multi-layer plasmonic devices and metamaterials," J. Opt. Soc. Am. A **31**, 1820–1831 (2014).
18. A. Schadle, L. Zschiedrich, S. Burger, R. Klose, and F. Schmidt, "Domain decomposition method for Maxwell's equations: scattering off periodic structures," J. Comput. Phys. **226**, 477–493 (2007).
19. G. Demesy, F. Zolla, A. Nicolet, and M. Commandre, "Versatile full-vectorial finite element model for crossed gratings," Opt. Lett. **34**, 2216–2219 (2009).
20. M. Huber, J. Schoberl, A. Sinwel, and S. Zaglmayr, "Simulation of diffraction in periodic media with a coupled finite element and plane wave approach," SIAM J. Sci. Comput. **31**, 1500–1517 (2009).
21. K. Stannigel, M. Konig, J. Niegemann, and K. Busch, "Discontinuous Galerkin time-domain computations of metallic nanostructures," Opt. Express **17**, 14934–14947 (2009).
22. D. Christensen and D. Fowers, "Modeling SPR sensors with the finite-difference time-domain method," Biosens. Bioelectron. **11**, 677–684 (1996).
23. H. Sai, Y. Kanamori, K. Hane, and H. Yugami, "Numerical study on spectral properties of tungsten one-dimensional surface-relief gratings for spectrally selective devices," J. Opt. Soc. Am. A **22**, 1805–1813 (2005).
24. N. C. Lindquist, T. W. Johnson, D. J. Norris, and S.-H. Oh, "Monolithic integration of continuously tunable plasmonic nanostructures," Nano Lett. **11**, 3526–3530 (2011).
25. D. Colton and R. Kress, *Inverse Acoustic and Electromagnetic Scattering Theory*, 2nd ed. (Springer-Verlag, 1998).
26. F. Reitich and K. Tamma, "State-of-the-art, trends, and directions in computational electromagnetics," Comput. Model. Eng. Sci. **5**, 287–294 (2004).
27. L. Greengard and V. Rokhlin, "A fast algorithm for particle simulations," J. Comput. Phys. **73**, 325–348 (1987).
28. D. P. Nicholls, "A method of field expansions for vector electromagnetic scattering by layered periodic crossed gratings," J. Opt. Soc. Am. A **32**, 701–709 (2015).
29. H. Kurkcu and F. Reitich, "Stable and efficient evaluation of periodized Green's functions for the Helmholtz equation at high frequencies," J. Comput. Phys. **228**, 75–95 (2009).
30. A. Barnett and L. Greengard, "A new integral representation for quasi-periodic scattering problems in two dimensions," BIT Numer. Math. **51**, 67–90 (2011).
31. O. Bruno, S. Shipman, C. Turc, and S. Venakides, "Efficient evaluation of doubly periodic Green functions in 3D scattering, including Wood anomaly frequencies," arXiv:1307.1176 (2013).
32. L. Rayleigh, "On the dynamical theory of gratings," Proc. R. Soc. London A **79**, 399–416 (1907).
33. S. O. Rice, "Reflection of electromagnetic waves from slightly rough surfaces," Commun. Pure Appl. Math. **4**, 351–378 (1951).
34. O. P. Bruno and F. Reitich, "Numerical solution of diffraction problems: a method of variation of boundaries," J. Opt. Soc. Am. A **10**, 1168–1175 (1993).
35. O. P. Bruno and F. Reitich, "Numerical solution of diffraction problems: a method of variation of boundaries. II. Finitely conducting gratings, Padé approximants, and singularities," J. Opt. Soc. Am. A **10**, 2307–2316 (1993).
36. O. P. Bruno and F. Reitich, "Numerical solution of diffraction problems: a method of variation of boundaries. III. Doubly periodic gratings," J. Opt. Soc. Am. A **10**, 2551–2562 (1993).
37. D. P. Nicholls and F. Reitich, "Shape deformations in rough surface scattering: cancellations, conditioning, and convergence," J. Opt. Soc. Am. A **21**, 590–605 (2004).
38. D. P. Nicholls and F. Reitich, "Shape deformations in rough surface scattering: improved algorithms," J. Opt. Soc. Am. A **21**, 606–621 (2004).
39. D. P. Nicholls and F. Reitich, "Boundary perturbation methods for high-frequency acoustic scattering: shallow periodic gratings," J. Acoust. Soc. Am. **123**, 2531–2541 (2008).
40. A. Malcolm and D. P. Nicholls, "A field expansions method for scattering by periodic multilayered media," J. Acoust. Soc. Am. **129**, 1783–1793 (2011).
41. P. Nagpal, N. C. Lindquist, S.-H. Oh, and D. J. Norris, "Ultrasmooth patterned metals for plasmonics and metamaterials," Science **325**, 594–597 (2009).

42. R. Petit, ed., *Electromagnetic Theory of Gratings* (Springer-Verlag, 1980).
43. D. P. Nicholls and F. Reitich, “A new approach to analyticity of Dirichlet-Neumann operators,” Proc. R. Soc. Edin. A **131**, 1411–1433 (2001).
44. D. P. Nicholls and F. Reitich, “Analytic continuation of Dirichlet-Neumann operators,” Numer. Math. **94**, 107–146 (2003).
45. R. W. Wood, “On a remarkable case of uneven distribution of light in a diffraction grating spectrum,” Philos. Mag. **4**(21), 396–402 (1902).
46. D. Gottlieb and S. A. Orszag, *Numerical Analysis of Spectral Methods: Theory and Applications*, Vol. **26** of CBMS-NSF Regional Conference Series in Applied Mathematics (Society for Industrial and Applied Mathematics, 1977).
47. D. P. Nicholls and F. Reitich, “Stability of high-order perturbative methods for the computation of Dirichlet-Neumann operators,” J. Comput. Phys. **170**, 276–298 (2001).
48. G. A. Baker, Jr. and P. Graves-Morris, *Padé Approximants*, 2nd ed. (Cambridge University, 1996).
49. C. M. Bender and S. A. Orszag, *Advanced Mathematical Methods for Scientists and Engineers*, International Series in Pure and Applied Mathematics (McGraw-Hill, 1978).
50. A. Rakic, A. Djurisic, J. Elazar, and M. Majewski, “Optical properties of metallic films for vertical-cavity optoelectronic devices,” Appl. Opt. **37**, 5271–5283 (1998).